Digital Object Identifier (DOI): 10.1109/TIA.2013.2240644

IEEE

Reactive power influence on the thermal cycling of multi-MW wind power inverter

Ke Ma
Marco Liserre
Frede Blaabjerg

Suggested Citation

Ma, K., Liserre, M. & Blaabjerg, F. “Reactive power influence on the thermal cycling of multi-MW wind power inverter,” apr 2013 I : I E E E Transactions on Industry Applications. 49, 2, s. 922-930 8 s.

Reactive Power Influence on the Thermal Cycling of Multi-MW Wind Power Inverter

Ke Ma[1], Marco Liserre[2], Frede Blaabjerg[1]

[1] Department of Energy Technology, Aalborg University
Pontoppidanstraede 101, DK-9220 Aalborg East, Denmark
kema@et.aau.dk, fbl@et.aau.dk

[2] Dept of Electrotechnical and Electronic Engineering, Polytechnic of Bari
Via E.Orabona 4, 70125 - Bari, Italy
liserre@poliba.it

***Abstract*—In this paper the reactive power influence on the thermal cycling of power devices in grid-connected inverter for 10 MW wind turbines is investigated. Restrained by the grid codes, the allowable reactive power ranges in relation to amplitude and phase angle of the load current for a single converter system are first presented at different wind speeds. Furthermore, the interaction between paralleled converter systems in a wind park is also considered and analyzed. By controlling the reactive power circulated among paralleled converters, a new concept is then proposed to stabilize the thermal fluctuation of the power devices during wind gusts. It is concluded that the reactive power may change the thermal distribution of power devices. By properly controlling the reactive power, it is possible to achieve a more stable junction temperature in the power devices during the fluctuation of wind speed, and thereby could provide a new way to improve the reliability of the wind power conversion system.**

I. INTRODUCTION

The European Union has committed itself to source 20% of its energy from renewables by 2020 [1]. As the most promising candidate, the wind energy production integrated into the power grid is booming up all over the world. Meanwhile, the power capacity of a single wind turbine is increasing continuously to reduce the price pr. produced kWh, as the cutting-edge achievement, 7 MW offshore wind turbines have already been presented on the market [2]-[4]. Consequently, due to much more significant impacts to the power grid than ever before, the wind power generation system is required to be more reliable and able to withstand some environment [5], [6] or grid disturbances [7].

The growing requirements for reliability and grid integration push the solutions of wind power generation system from Doubly Fed Induction Generator (DFIG) with partial-rated power converter to Synchronous or Asynchronous Generator with full-scale power converter. In the full-scale power converter solutions, there are more flexibilities to control the reactive power, and it is easier to satisfy the grid voltage support requirements by most of the grid standards under both normal and faults condition of the power grid [8]-[10].

However, the added reactive power, especially in the application of multi-MW wind power conversion, may increase the converter output voltage (modulation index) and change the amplitude as well as phase angle of the load current in the grid side inverter, as shown in Fig. 1. The voltage and current phasor diagram from the point view of power grid by introducing the overexcited and underexcited reactive current I_Q in grid connected converter are indicated respectively. More detail definitions for the overexcited and underexcited operation are specified in [10]. Referring to the

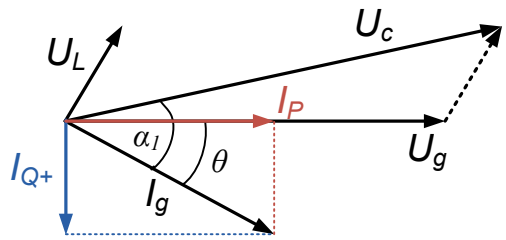

(a) Receive overexcited reactive power from converter (I_{Q+}).

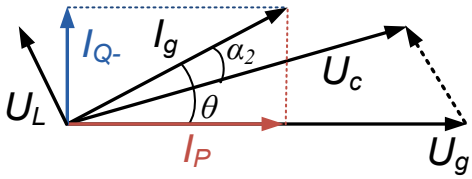

(b) Generate underexcited reactive power to converter (I_{Q-}).

Fig. 1. The phasor diagram from the power grid point of view by introducing reactive power in grid converter (U_c represents the converter output voltage, U_g grid voltage, U_L voltage drop on filter inductor, I_g load current, I_P active current, I_Q reactive current, $cos\theta$ power factor, α the phase angle).

commonly used and accepted loss model in [11]-[12], the modified output voltage and load current will change the loss consumption and distribution, and thereby lead to the change of thermal cycling (or junction temperature) of power switching devices. According to most of the reliability models for power semiconductors [13]-[16], the life time of the wind power inverter is closely related to the thermal cycling performance-both average mean junction temperature and temperature fluctuation amplitude, therefore it is interesting to investigate the relationship between the reactive power and the resulting modified thermal cycling for multi-MW wind power inverters.

In this paper, the allowable reactive power ranges as well as their impacts on thermal cycling of wind power inverters are presented at different wind speeds. The situations when considering single converter and paralleled converter systems in a wind park are analyzed respectively. A new concept is also proposed to stabilize the device thermal fluctuation during wind gust by controlling the reactive power circulated among parallel converter systems in a wind park.

II. Effect of Reactive Power in Case of Single Converter

As the most commercialized multilevel topology which is widely used in the high-power medium-voltage drives for industry, mining, and traction applications [17], [18], the three-level neutral-point-clamped (3L-NPC) converter seems to be a promising candidate for the Multi-MW full-scale wind power conversion system [19]-[21], as shown in Fig. 2. This converter is chosen and basically designed based on a 10 MW wind turbine as a case study [19], [20], [22], where the major design parameters are summarized in Table I.

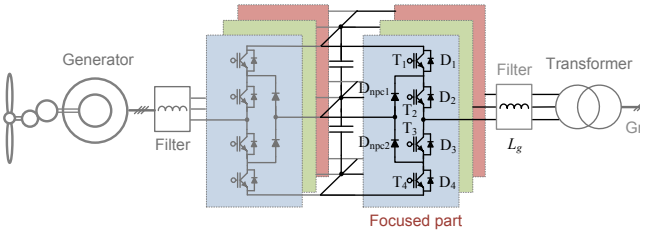

Fig. 2. Three-level Neutral point clamped converter used in a wind turbine.

Table I. Parameters of three-level Neural Point Clamped inverter for case study

Rated active power P	10 *MW*
DC bus voltage V_{dc}	5.6 *kV DC*
[1]Rated primary side voltage V_{ll}	3.3 *kV rms*
[2]Rated phase current I_{phase}	1.94 *kA rms*
Carrier frequency f_c	800 *Hz*
Filter inductance L_f	1.13 *mH* (0.3 *p.u.*)

1. Line-to-line voltage in the primary windings of the transformer.
2. Phase current when power factor is 0.9.

For a single wind power generation system, the maximum reactive power achieved by the grid side inverter has to be restrained in a certain range according to the grid standards [8]-[10], as shown in Fig. 3, in which the allowable boundaries of reactive power with relation to the generating active power is defined by German grid code when the grid voltage is within ±5% range around nominal value. It can be seen that in the definition of Variant 1 the overexcited reactive power Q_+ should be less than 48% of the rated active power P_{rated}, and the underexcited reactive power Q- should be less than 23% of P_{rated}.

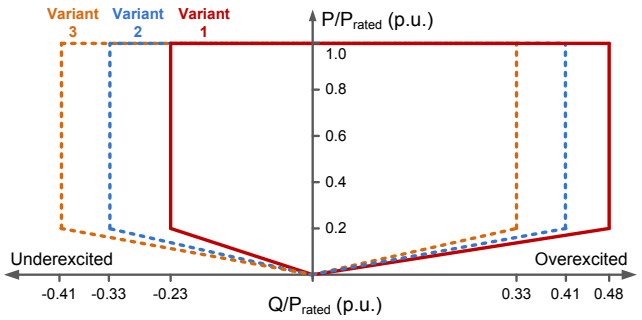

Fig. 3. The P, Q range of wind power converter during normal operation defined by the German grid codes [8].

Referring to the phasor diagram of the grid side converter in Fig. 1, the amplitude of the load current I_g with relation to the reactive power Q and active power P can be calculated as:

$$I_g = \frac{\sqrt{P^2 + Q^2}}{3 \cdot U_g} \tag{1}$$

Where U_g is the rms value of grid phase voltage. The phase angle α between load current I_g and converter output voltage U_c in Fig. 1 can be calculated as:

$$\alpha_1 = \arctan\left[\frac{U_g \cdot \sin\theta + 2\pi f_o L_f \cdot I_g}{U_g \cdot PF}\right] \tag{2}$$

when introducing overexcited reactive power, and

$$\alpha_2 = -\arctan\left[\frac{U_g \cdot \sin\theta - 2\pi f_o L_f \cdot I_g}{U_g \cdot PF}\right] \tag{3}$$

when introducing underexcited reactive power.

In (2) and (3), the power factor angle θ is:

$$\theta = \arccos\frac{P}{\sqrt{P^2 + Q^2}} \tag{4}$$

Referring to the grid code defined in Fig. 3, the restrained condition has to be added as:

$$-0.23P \le Q \le 0.48P \tag{5}$$

given the condition that the power factor are maintained and generating active power P is larger than 20% of its rated value.

Then the amplitude and phase angle of the load current I_g in relation to the reactive power p.u. can be plotted in Fig. 4 (a) and Fig. 4 (b) respectively, in which the situations when the wind speed is 12 m/s (P = 10 MW, 1 p.u.), 10 m/s (P = 6.3 MW, 0.63 p.u.), and 8 m/s (P = 3.2 MW, 0.32 p.u.) are indicated.

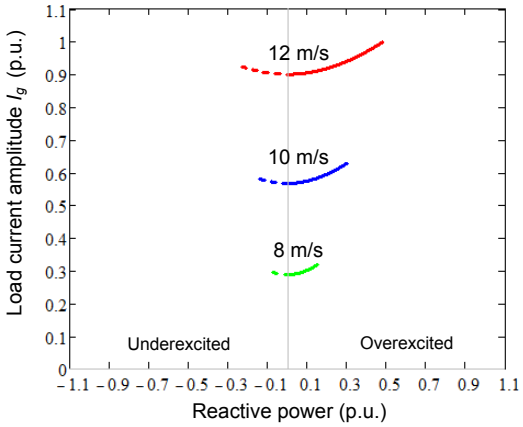

(a) Current amplitude I_g vs. reactive power Q

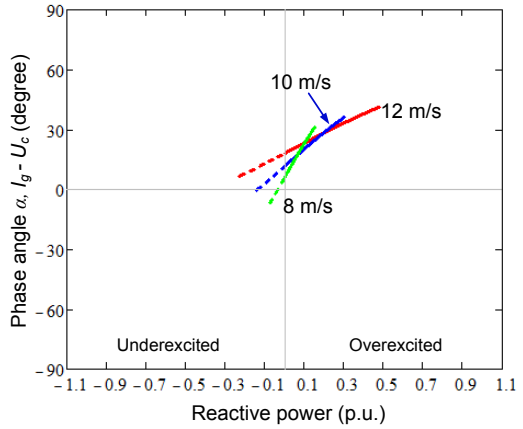

(b) Phase angle α vs. reactive power Q

Fig. 4. Load current vs. reactive power when complying with grid codes (dot line represents underexcited Q_-, real line represents overexcited Q_+).

In order to investigate the maximum impact of the reactive power to the losses and find the thermal distribution of the power devices, three extreme conditions when complying with grid codes are chosen based on 10 m/s wind speed from Fig. 4 (10 m/s is the typical average annual offshore wind speed defined by IEC I wind class standard [23]): the maximum underexcited reactive power boundary when $Q_{-max\ (10\ m/s)}$ = -0.13 p.u., no reactive power when PF = 1, and maximum overexcited reactive power boundary when $Q_{+max\ (10\ m/s)}$ = 0.27 p.u..

The loss model shares the same idea in [11], [12], which is a commonly accepted method for loss evaluation of power semiconductor devices, the conduction loss and switching loss are accumulated by switching cycles according to the information of conduction voltage as well as switching energy in relation to the load current provided by the datasheets of manufacturers. The simulation is carried out based on PLECS Blockset in Simulink [24]. Press-pack IGCT 5SHY35L4512 (commutated voltage 2.8 kV/ maximum current 3.3 kArms) and diodes 5SDF16L4503 (2.8 kV/2.6 kArms) from ABB [25] are chosen as the power switching devices. For simplicity losses dissipated in the devices are considered as temperature independent.

The thermal models of a single switch and clamped diode are indicated in Fig. 5 [14], [25]-[27], in which the thermal impedance from junction to case $Z_{(j\text{-}c)}$ is modeled as a four-layers Foster RC network, as shown in Fig. 6. Each of the thermal parameters can be found from the manufacturer datasheets and they are summarized in Table II, where the thermal resistance R_{th} will decide the steady state mean value of junction temperature, and the thermal capacitance (with time constant τ) will decide the dynamic change or fluctuation of the junction temperature. The ambient temperature is set to 50 ℃ and considered constant during the operation of converter, however it may be changed depending on the operation site.

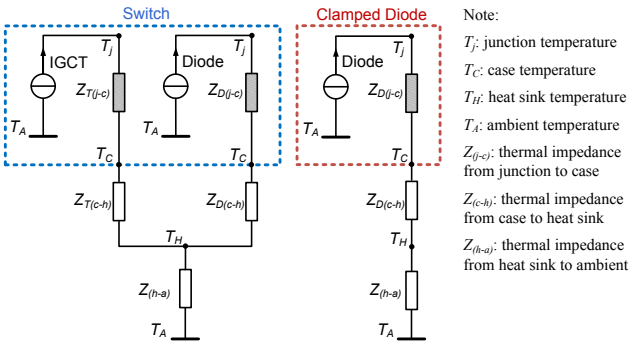

Fig. 5. Thermal models of the power devices.

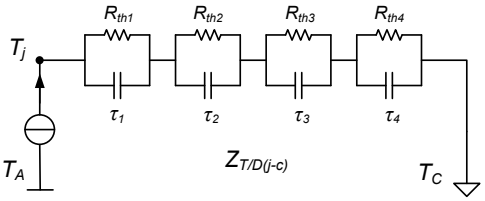

Fig. 6. Thermal model of the impedance $Z_{T(j\text{-}c)}$ or $Z_{D(j\text{-}c)}$ from junction to case in Fig. 5.

Table II. Parameters of thermal impedance for IGCT/diode.

Thermal Impedance	$Z_{T/D(j\text{-}c)}$				$Z_{T/D(c\text{-}h)}$
	Sector 1	Sector 2	Sector 3	Sector 4	
R_{iIGCT} (K/kW)	5.562	1.527	0.868	0.545	3
τ_{iIGCT} (s)	0.5119	0.896	0.0091	0.0024	-
R_{iDiode} (K/kW)	11.124	3.054	1.736	1.09	6
τ_{iDiode} (s)	0.5119	0.896	0.0091	0.0024	-

*Sector N means different layers of thermal RC lump in Fig. 6.

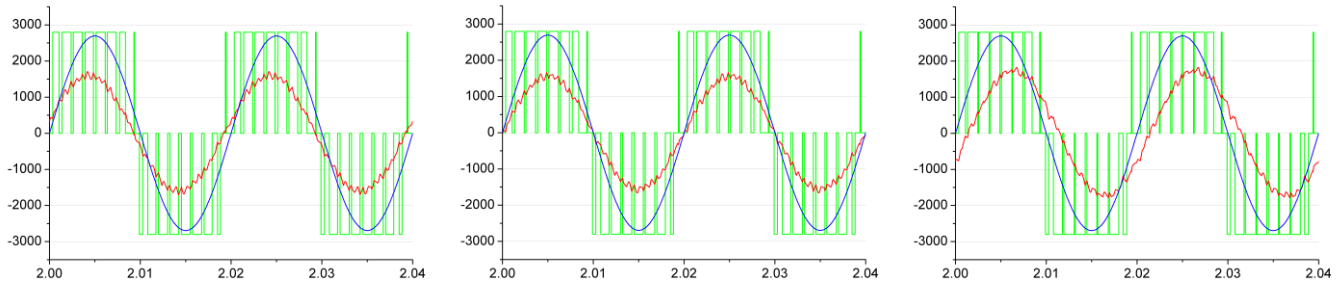

(a) Q_{-max}=-0.13 p.u. (b) Q=0 p.u. (c) Q_{+max}=0.27 p.u.

Fig. 7. Output waveforms of 3L-NPC inverter under different reactive power (boundaries defined by grid codes, 10 m/s wind speed), output voltage pulses (Green), grid voltage (blue), phase current (red).

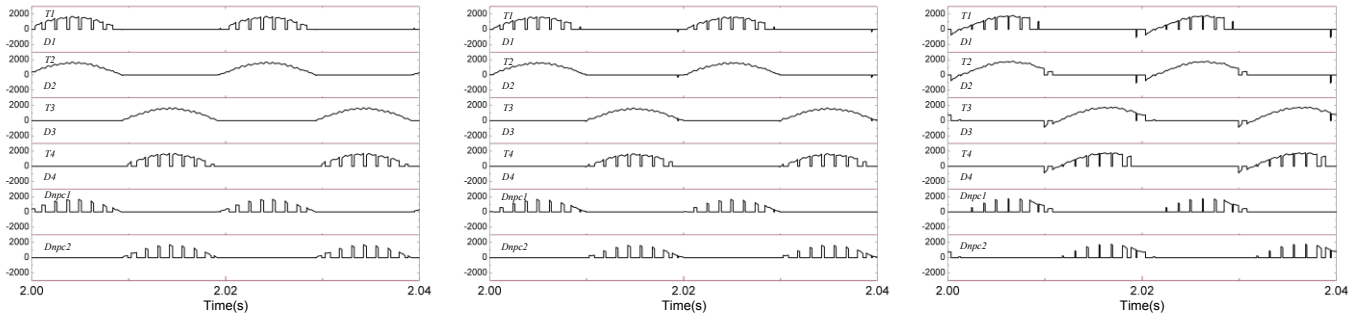

(a) Q_{-max}=-0.13 p.u. (b) Q=0 p.u. (c) Q_{+max}=0.27 p.u.

Fig. 8. Current distribution of 3L-NPC inverter under different reactive powers (boundaries defined by grid codes, 10 m/s wind speed).

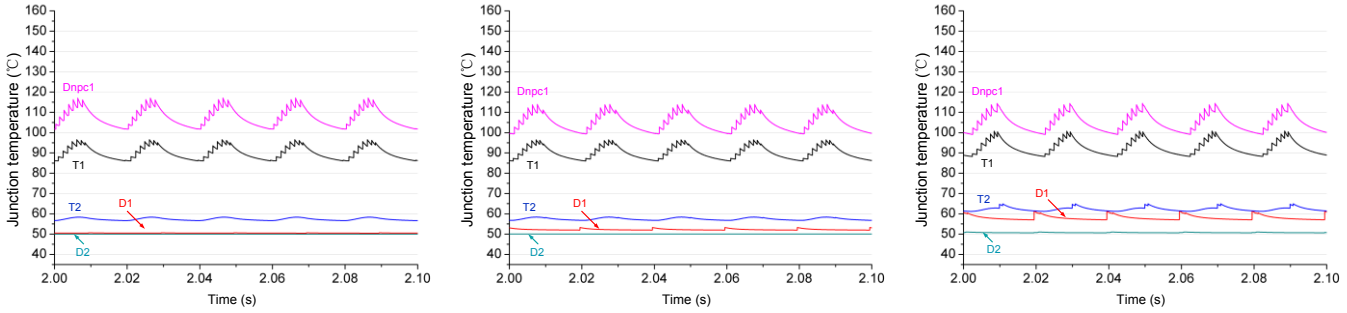

(a) Q_{-max}=-0.13 p.u. (b) Q=0 p.u. (c) Q_{+max}=0.27 p.u.

Fig. 9. Thermal cycling of 3L-NPC inverter under different reactive powers (boundaries defined by grid codes, 10 m/s wind speed).

It is noted that the separately packaged IGCT and diodes are chosen because of the limitation for available products which can be found on the market. However, in a practical converter design, the IGCT/IGBT and its freewheeling diode are usually integrated and packaged together, the chip size for diode is about half of that for the IGCT/IGBT, accordingly, the thermal resistance of the diode from junction to heat sink is not consistent with its datasheet values but set to twice of the IGCT.

It is also noted that the thermal impedance between heat sink and ambient $Z_{(h\text{-}a)}$ in Fig. 5 is closely related to the design of the heat sink and of the layout for the power devices, which are application-dependent and they are out of the scope of this paper, therefore the $Z_{(h\text{-}a)}$ is not included in the thermal analysis. However, it is worth mentioned that, the cost and structure of heatsink system do have impacts to the thermal impedance and temperature profile of power devices [28]. If heatsinks with small thermal resistance and large thermal capacitance are used, normally the temperature rise on the heat sink has smaller amplitude and longer time constant compared to the temperature rise inside the power devices. After the heat sink system is chosen and optimized, the temperature rise on the heat sink will be known and it is possible to be included in the analysis.

The simulation results regarding inverter outputs and current distribution are shown in Fig. 7 and Fig. 8 respectively, where the three extreme reactive power conditions are introduced to the inverter when generating 0.63 p.u. active power at 10 m/s wind speed. It can be seen that when complying with the regulations by grid codes, the differences of converter outputs with the given three extreme reactive powers are insignificant.

The loss simulation results of the 3L-NPC wind power inverter are presented in Fig. 10, in which three given reactive power conditions are compared. It can be seen that there is no significant loss difference between the three conditions where different amount of reactive power are introduced. The situation at the maximum overexcited reactive power boundary (Q_{+max} = 0.27 p.u.) consumes slightly more loss in the outer switches and diode T1, D1 and inner switch T2 of the 3L-NPC inverter.

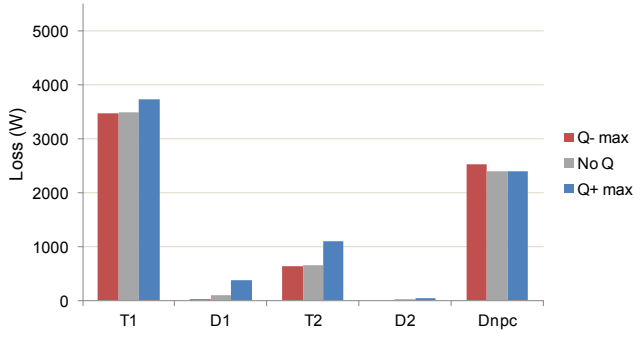

Fig. 10. Loss distribution of 3L-NPC inverter with different extreme reactive powers (Complying with grid codes).

According to the junction temperature simulation results in Fig. 9, the thermal cycling in the most stressed devices of the clamping diode Dnpc as well as the outer switches T1 has no significant difference among the three reactive power operating points.

III. Effect of Reactive Power in Case of Paralleled Converters

For wind power converter systems in a wind farm, the grid side inverters are connected as a local grid, therefore the reactive power can basically be circulated among the inverters locally and not necessarily be seen in the power grid, as shown in Fig. 11. It can be seen that the underexcited reactive power $-Q$ absorbed by converter 1 is generated/compensated by the converter 2 which is under overexcited operation with $+Q$,

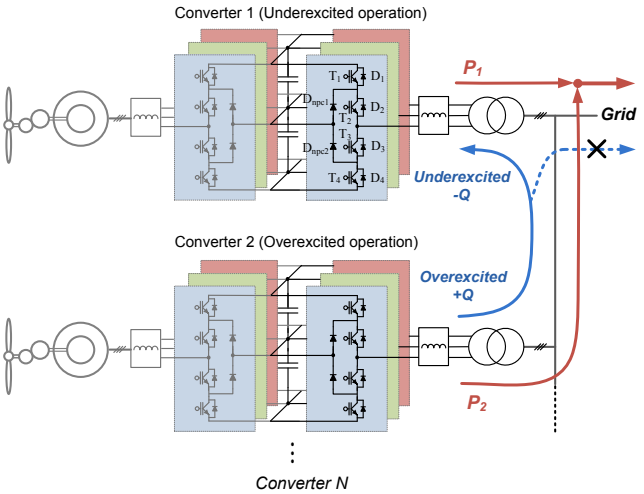

Fig. 11. Reactive power circulated in paralleled wind power converters.

and there is no (or less) reactive power injected into the power grid. On this condition the operation range of reactive power in converter 1 and converter 2 is not restrained by the grid codes but by the amplitude of load current as well as the converter output voltage, which is due to the limitations of device current rating and maximum modulation index of the power converter.

The new ranges of amplitude and phase angle of the load current with relation to the reactive power are shown in Fig. 12, which is restrained by:

$$-\sqrt{S^2-P^2} \le Q \le \sqrt{S^2-P^2} \tag{6}$$

$$M \le 1 \tag{7}$$

where the modulation index M can be calculated as:

$$M = \frac{\sqrt{6}\cdot U_c}{V_{dc}} = \frac{\sqrt{6}\cdot\sqrt{(U_g\cdot PF)^2+[U_g\cdot\sin\theta \pm 2\pi f_o\cdot L_f\cdot I_g]^2}}{V_{dc}} \tag{8}$$

It can be seen that the operating range of reactive power is significantly extended compared to Fig. 4, and the ranges for overexcited and underexcited reactive current are

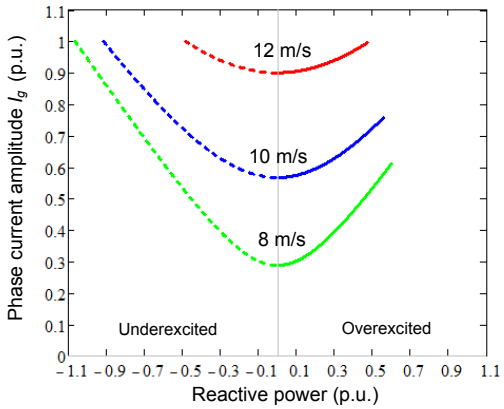

(a) Current amplitude I_g vs. reactive power Q

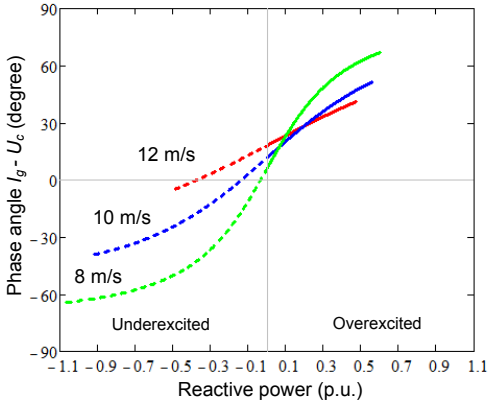

(b) Phase angle α vs. reactive power Q

Fig. 12. Operation range of reactive power when complying with grid codes (dot line represents underexcited Q_-, real line represents overexcited Q_+).

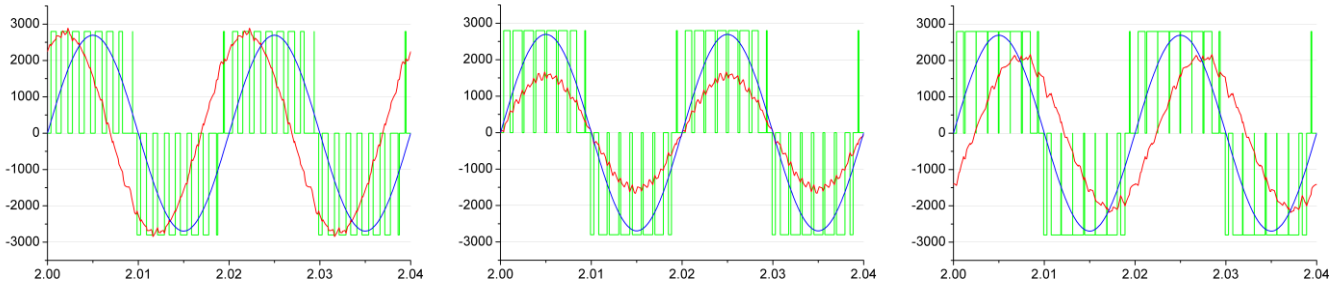

(a) Q_{-max}=-0.82 p.u. (b) Q=0 p.u. (c) Q_{+max}=0.55 p.u.

Fig. 13. Output waveforms of 3L-NPC inverter under different reactive power (Considering interaction of inverters, 10 m/s wind speed), output voltage pulses (Green), grid voltage (blue), phase current (red).

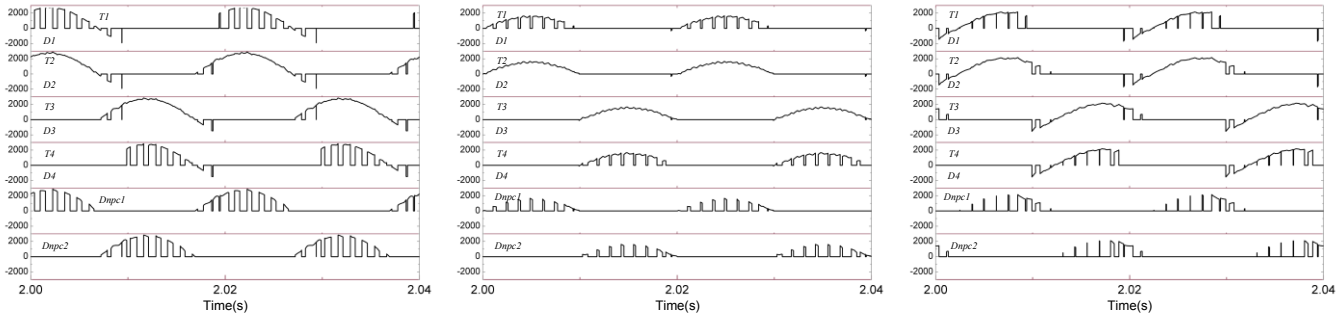

(a) Q_{-max}=-0.82 p.u. (b) Q=0 p.u. (c) Q_{+max}=0.55 p.u.

Fig. 14. Current distribution of 3L-NPC inverter under different reactive powers (Considering interaction of inverters, 10 m/s wind speed).

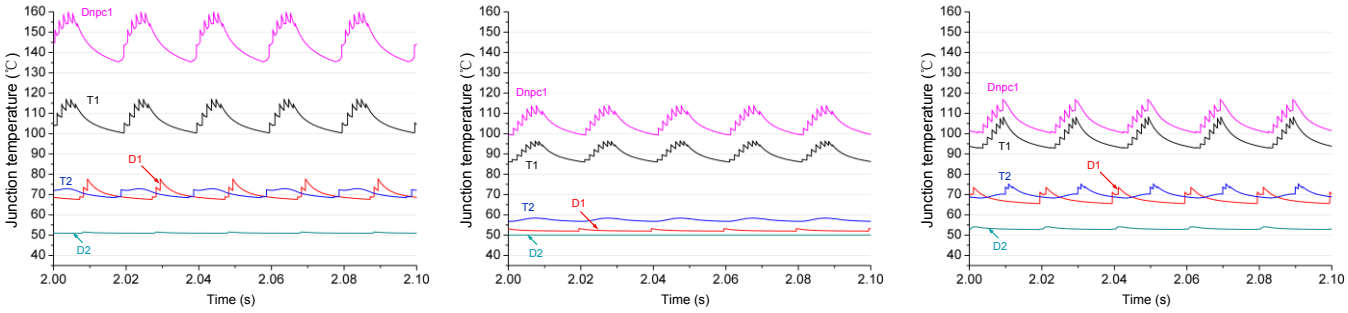

(a) Q_{-max}=-0.82 p.u. (b) Q=0 p.u. (c) Q_{+max}=0.55 p.u.

Fig. 15. Thermal cycling of 3L-NPC inverter under different reactive powers (Considering interaction of inverters, 10 m/s wind speed).

unsymmetrical: The increase of Q_+ will cause an increase of converter output voltage U_c, therefore the Q_+ is first limited by the maximum modulation index before it gets to the limitation of maximum device current rating. While the increase of Q_- will cause a decrease of U_c and the modulation index, therefore Q_- is only limited by the device current rating.

Another three extreme reactive power conditions when considering the interaction between paralleled converters are investigated based on 10 m/s wind speed: the maximum underexcited reactive power boundary when $Q_{-max\ (10m/s)}$=-0.82 p.u., no reactive power when PF=1, and maximum overexcited reactive current boundary when $Q_{+max\ (10\ m/s)}$=0.5 p.u..

The simulation results regarding inverter outputs and current distribution are shown in Fig. 13 and Fig. 14 respectively, where the three extreme reactive power conditions are introduced when generating 0.63 p.u. active power at 10 m/s wind speed. It can be seen that when considering the interaction between paralleled converters, the converter output pulse width, amplitude and phase angle of load current with the given three extreme reactive powers significantly differ from each other.

The loss simulation results are presented in Fig. 16, in which three given reactive power conditions are compared when the interaction between parallel converters are considered. It can be seen that the situation at maximum overexcited reactive power boundary (Q_{+max} =0.55 p.u.) consumes significant more loss than the situation without reactive power in the outer switch T1, outer diode D1, inner switch T2 and clamping diode D_{npc} of the 3L-NPC inverter. The major difference between overexcited and underexcited

reactive power boundary is at the stress of the clamping diode, the later has much less loss than the former one in Dnpc.

According to the junction temperature simulation results in Fig. 15, the thermal cycling of the most stressed device of the clamping diode Dnpc as well as outer switch T1 is significant higher than the other two reactive power operating points.

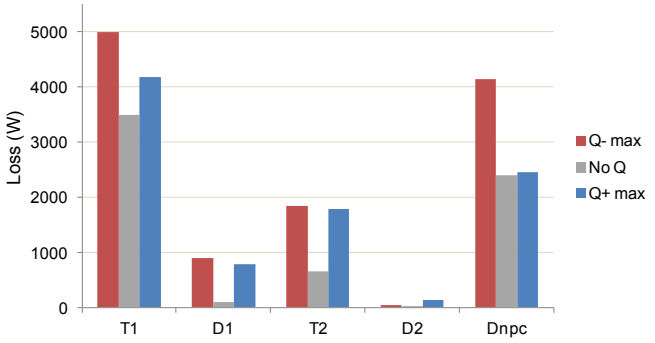

Fig. 16. Loss distribution of 3L-NPC inverter with different extreme reactive powers (Considering parallel converters).

in this paper the operation conditions of converter with various reactive powers are analyzed based on p.u. system, with other converter ratings and designs the basic operation status e.g. current loading and voltage outputs will be similar except for the switching frequency. Due to different parameters for loss and thermal models, the loss and junction temperature profile could deviate from the results obtained in this paper if other power devices are applied. However, according to the device current loadings in Fig. 14, the extreme underexcited operation of converter will further increase the stress of D_{npc} no matter which device is the adopted, because the extreme underexcited operation lead to much higher current amplitude with more conduction time of D_{npc}. The extreme overexcited operation of converter will further increase the stress of T_1 for the same reasons.

IV. Reactive Power Control Method to Stablize the Thermal Cycling

It can be seen that when considering the interaction among paralleled inverters, the underexcited reactive power operation may introduce significantly increased junction temperature to the most stressed devices of 3L-NPC inverter (outer switches T_1 and clamping diode D_{npc}). This feature can be utilized to heat up the power devices in a proper manner during load changes, e.g. wind gust. Thereby the fluctuation of junction temperature ΔT_j during load changes can be stabilized. (ΔT_j is claimed be more harmful to the reliability of the power switching devices compared to the average mean junction temperature T_{jm}, as indicated in [13]-[16]).

According to the one year return period wind gust definition by IEC standards [23], a wind gust condition with different reactive current references for a case study is indicated in Fig. 17 (the wind speed is set from 10 m/s dropping to 8 m/s and rising to 16 m/s, then the reverse fashion is continued). The active current reference of the converter is accordingly changed with the wind speed referring to the wind turbine model in [29], while the reactive power references are different:

Fig. 17 (a) is the situation without any reactive current during the wind gust. Fig. 17 (b) is the condition for converter 1 in Fig. 11 which enables the junction temperature stabilization control: the amount of underexcited reactive current is adjusted to keep the mean value of junction

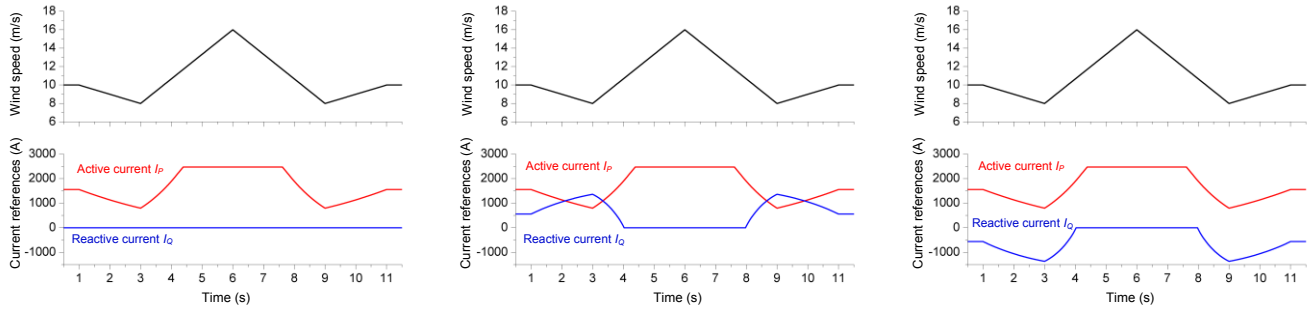

(a) Without reactive power (b) With underexcited reactive power (c) With overexcited reactive power

Fig. 17. Wind gust and current references of 3L-NPC inverter for case study.

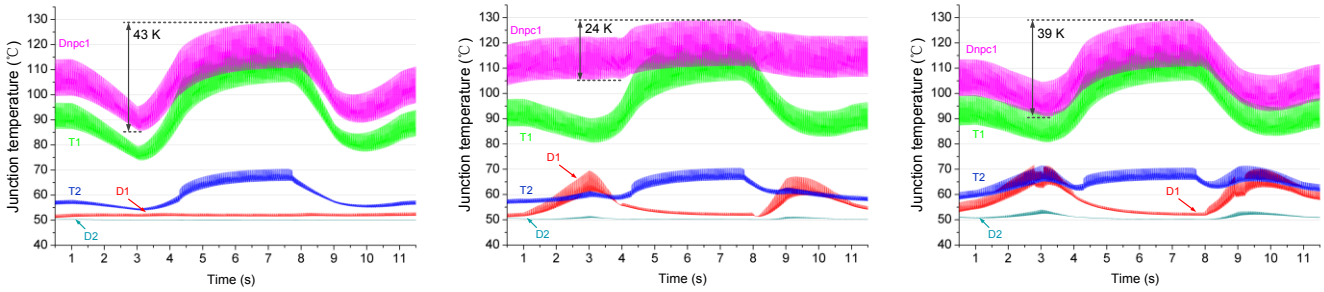

(a) Without reactive power (b) With underexcited reactive power (c) With overexcited reactive power

Fig. 18. Thermal cycling of 3L-NPC inverter during wind gust.

temperature in the most stressed device (Dnpc) constant when the wind speed is below 11 m/s, and the reactive current is kept zero when the wind speed is above 11 m/s to avoid over heat of the most stress device. The basic idea and used models for calculating the active and reactive current references is shown in Fig. 19.

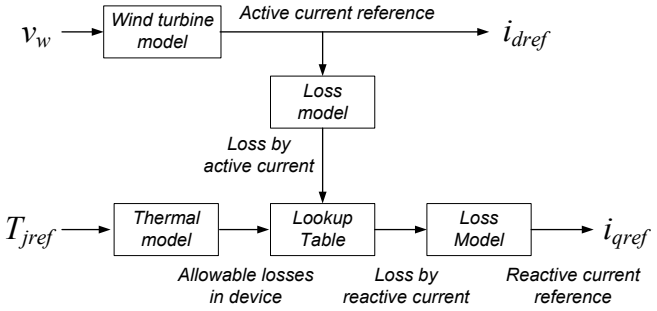

Fig. 19. The basic idea and used models for calculating the active and reactive current references of Fig. 18 (b). (v_w is the wind speed, T_{jref} is the target junction temperature mean value to be stablized in the most stressed devices.)

Fig. 17 (c) shows the situation for converter 2 in Fig. 11 which enables the reactive power compensation control: The amount of overexcited reactive current is adjusted to generate the underexcited reactive power consumed by the converter 1. As a result the overexcited reactive current reference in Fig. 17 (c) has the same amplitude but opposite direction compared to Fig. 17 (b). In Fig. 17 (b) and (c) the maximum reactive power during wind gust is around ± 0.55 p.u., which is limited by the modulation index in the converter 2 for reactive power compensation. However this limit can be extended by considering more paralleled converters in a wind farm.

The junction temperature distribution of the target 3L-NPC inverter with different reactive current control strategies are indicated in Fig. 18. It is obvious that the thermal fluctuations in the most stressed devices (clamping diode Dnpc) are significantly reduced from 43 K in Fig. 18 (a) without reactive power to 24 K in Fig. 18 (b) with the junction temperature stabilization control. It can be seen that when introducing the reactive power compensation in paralleled converter 2 with overexcited reactive current, the maximum junction temperature of the most stressed devices Dnpc in Fig.18 (c), is not further more increased.

However, when introducing reactive power (either overexcited or underexcited) to the 3L-NPC inverter, the outer diode D1, inner switch T2 inner diode D2 are slightly more stressed compared to the situation without any reactive power control.

It is noted that the reactive power is only circulated inside parallel converters in order to heat up the power switching devices and is not injected into the power grid, the target of the proposed reactive power control method is different from the regular one used to support the grid voltage. However, the operation modes and reactive power controls of converter can be switched depending on the grid condition in the real system.

CONCLUSIONS

The introduction of reactive current may change the thermal distribution of power devices. The operation ranges of reactive current not only depend on the grid codes, but also relate to the interaction between paralleled inverters -the latter situation has much wider allowable reactive current range than the former one.

By introducing reactive current during the lower wind speed of a wind gust, the junction temperature fluctuation in the most stressed devices of a 3L-NPC wind power inverter can be significantly stabilized, and the reliability could thereby be improved according to e.g. the Coffin-Masson life time models, while the increased stresses to the other devices or paralleled converters are still acceptable.

The control strategies for junction temperature stabilization by reactive power are still open questions needed to be further investigated. They are closely related to the wind gust conditions, wind farm configurations, as well as grid codes requirements, etc. All of these factors will change the behavior of reactive power cycling among parallel converters in a wind farm.

REFERENCES

[1] European Commission Climate Action, "The EU climate and energy package", March 2007.

[2] F. Blaabjerg, Z. Chen, S.B. Kjaer, "Power Electronics as Efficient Interface in Dispersed Power Generation Systems", *IEEE Trans. on Power Electronics*, 2004, vol. 19, no. 4, pp. 1184-1194.

[3] Z. Chen, J.M. Guerrero, F. Blaabjerg, "A Review of the State of the Art of Power Electronics for Wind Turbines," *IEEE Trans. on Power Electronics,* vol.24, no.8, pp.1859-1875, Aug. 2009.

[4] Website of Vestas Wind Power, Wind turbines overview, April 2011. (Available: http://www.vestas.com/)

[5] T. Geyer, S. Schröder, "Reliability Considerations and Fault-Handling Strategies for Multi-MW Modular Drive Systems," *IEEE Trans. on Industrial Applications*, vol.46, no.6, pp.2442-2451, Nov.-Dec. 2010

[6] Pinjia Zhang, Yi Du, T.G. Habetler, Bin Lu, "A Survey of Condition Monitoring and Protection Methods for Medium-Voltage Induction Motors," *IEEE Trans. on Industrial Applications*, vol.47, no.1, pp.34-46, Jan.-Feb. 2011

[7] K. Ma, F. Blaabjerg, M. Liserre, "Thermal analysis of multilevel grid side converters for 10 MW wind turbines under Low Voltage Ride Through," in *Proc. of ECCE 2011*, pp. 2117 - 2124, Sep 2011.

[8] M. Altin, O. Goksu, R. Teodorescu, P. Rodriguez, B. Bak-Jensen, L. Helle, "Overview of recent grid codes for wind power integration," in *Proc. of OPTIM'2010*, pp.1152-1160, 2010.

[9] M. Tsili, S. Papathanassiou, "A review of grid code technical requirements for wind farms," *IET Renewable Power Generation*, vol.3, no.3, pp.308-332, 2009.

[10] E.ON-Netz – Grid Code. High and extra high voltage, April 2006.

[11] F. Blaabjerg, U. Jaeger, S. Munk-Nielsen and J. Pedersen, "Power Losses in PWM-VSI Inverter Using NPT or PT IGBT Devices," *IEEE Trans. on Power Electronics,* vol. 10, no. 3, pp. 358–367, May 1995.

[12] D. Graovac, M. Purschel, "IGBT Power Losses Calculation Using the Data-Sheet Parameters," Infineon Application Note, January, 2009.

[13] A. Wintrich, U. Nicolai, W. Tursky, T. Reimann, "Application manual power Semiconductors," Semikron Application Manual, Chapter 2.7 Reliability, 2011.
[14] W. Lixiang, J. McGuire,R.A. Lukaszewski, "Analysis of PWM Frequency Control to Improve the Lifetime of PWM Inverter," *IEEE Trans. on Industrial Applications,* vol. 47, no. 2, pp. 922-929, 2011.
[15] I.F. Kovačević, U. Drofenik, J.W. Kolar, "New physical model for lifetime estimation of power modules," in *Proc. IPEC'10*, pp. 2106-2114, 2010.
[16] N. Kaminski, "Load-Cycle Capability of HiPaks," ABB Application Note 5SYA 2043-01, Sep 2004.
[17] S. Kouro, M. Malinowski, K. Gopakumar, J. Pou, L. G. Franquelo, B. Wu, J. Rodriguez, M. A. Perez, J. I. Leon, "Recent Advances and Industrial Applications of Multilevel Converters," *IEEE Trans. on Power Electronics*, vol. 57, no. 8, pp. 2553 – 2580, 2010.
[18] J. Rodriguez, S. Bernet, P. K. Steimer, I. E. Lizama, "A Survey on Neutral-Point-Clamped Inverters," IEEE Transactions on Industrial Electronics, vol. 57, no. 7, pp. 2219-2230, 2010.
[19] F. Blaabjerg, M. Liserre, K. Ma, "Power Electronics Converters for Wind Turbine Systems," *IEEE Trans. on Industrial Applications*, 2012.
[20] K. Ma, F. Blaabjerg, "Multilevel Converters for 10 MW Wind Turbines," in *Proc. of EPE 2011*, pp. 1-8, August 2011.
[21] O.S. Senturk, L. Helle, S. Munk-Nielsen, P. Rodriguez, R. Teodorescu, "Power Capability Investigation Based on Electro-thermal Models of Press-pack IGBT Three-Level NPC and ANPC VSCs for Multi-MW Wind Turbines," *IEEE Trans. on Power Electronics*, 2012.
[22] H. Li, Z. Chen, H. Polinder, "Optimization of Multibrid Permanent-Magnet Wind Generator Systems," *IEEE Trans. on Energy Conversion,* vol. 24, no. 1, pp. 82-92, 2009.
[23] Wind turbines, part 1: Design requirements, IEC 61400-1, 3rd edition, International Electrotechnical Commission, 2005.
[24] User manual of PLECS blockset version 3.1, March 2011.
[25] Website of ABB semiconductors, Jan 2012 (Available on: http://www.abb.com/product/us/9AAC910029.aspx).
[26] B. Backlund, R. Schnell, U. Schlapbach, R. Fischer, "Applying IGBTs," ABB Application Note 5SYA2053-01, May 2007.
[27] O.S. Senturk, L. Helle, S. Munk-Nielsen, P. Rodriguez, R. Teodorescu, "Converter Structure-Based Power Loss and Static Thermal Modeling of The Press-Pack IGBT Three-Level ANPC VSC Applied to Multi-MW Wind Turbines," *IEEE Trans. on Industrial Applications,* vol. 47, no. 6, pp. 2505-2515, 2011.
[28] Dawei Xiang, Li Ran, P. Tavner, A. Bryant, Shaoyong Yang, P. Mawby, "Monitoring Solder Fatigue in a Power Module Using Case-Above-Ambient Temperature Rise," *IEEE Trans. on Industrial Applications*, vol.47, no.6, pp.2578-2591, Nov.-Dec. 2011.
[29] H.Polinder, F.F.A.van der Pijl, G.-J.de Vilder, P.J.Tavner, "Comparison of direct-drive and geared generator concepts for wind turbines," *IEEE Trans. on Energy Conversion*, vol. 21, no. 3, pp. 725-733, 2006.